2011 50th IEEE Conference on Decision and Control and
European Control Conference (CDC-ECC)
Orlando, FL, USA, December 12-15, 2011

Extracting Dynamics from Blur

Sandipan Mishra and John Wen

Abstract— **This paper considers dynamic state estimation using blurry measurements from image sensors such as CCD(charge coupled device) or CMOS(complementary metal oxide semiconductor) arrays. Typically, the information obtained from these sensors is the time-averaged output measurement during the exposure time. The additional information available in the intensity distribution, termed *blur*, is disregarded as noise. This manuscript models the image sensor as an integrative intensity sensor and exploits its unique properties to extract additional (non-linear) output information through spatial moments of the intensity distribution. An extended Kalman filter is then designed to exploit this information for better state reconstruction. We illustrate this modeling and algorithm development in the context of state estimation for adaptive optics systems. Simulation results verify that using the spatial moments can lead to more fidelous state estimation.**

I. Introduction

Image sensors are now prevalent as feedback measurement mechanisms for a wide variety of applications. Typical image sensors consist of an array of CMOS or CCD elements. The fundamental restriction of these systems is the update rate of these elements, which are limited to a few hundred Hz at best and more commonly around $15-50$ Hz. The image sensors deliver temporally integrated measurements over the exposure period, which are conventionally interpreted the *time-average* of the image feature of interest.

A typical vision-feedback system is usually a multi-rate system, with a fast-acting actuator and a slow image sensor. Using multi-rate techniques for identification, estimation, and control of image-feedback systems can certainly enhance closed-loop performance [1]. However, loop bandwidth will be still constrained by the fact that the image sensor provides limited information at a slow rate.

To overcome this seeming impasse, we exploit a unique feature of the image sensing array. A rapidly changing (or moving) image produces a blurry beam trace at the sensor. This *blur* is considered undesirable and is removed, assuming it to be "noise". However, this ignores (and destroys) a unique characteristic of the image sensor that it is an ***integrative intensity sensor***, i.e., the image sensor transforms temporal information about the motion of the object being imaged into a spatial intensity distribution. This extremely important property of the image sensor can in fact be used to *extract output time-history* and hence *reconstruct motion (output dynamics) during the exposure time*. Extraction of time-history at a fast-rate from the slow-rate integrative sensor promises to break the barrier of control bandwidths limited to frame update rates of the image sensor in applications that rely on image sensor feedback.

In image processing, *motion blur* [2] refers to the phenomenon observed when an image sensor captures relative motion of an object during the exposure time. Evolution of the output (object position) within a single exposure is codified through a *time-varying spatial point spread function* (PSF), which is temporally integrated by the image sensor. Figure 1 shows an image with motion blur and the corresponding deblurred image (taken from [3]). Motion blur has been the focus of research in both the image processing community as well as the visual perception community [4].

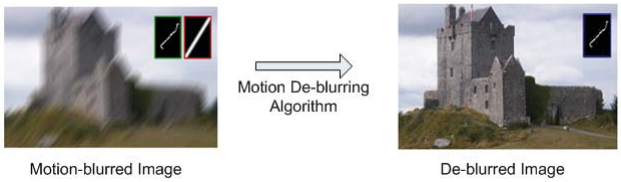

Fig. 1. Effect of relative motion between the camera and the object (left) (taken from [3]). The *blur* is because of the temporal integration of the sensor during exposure. Deblurring removes this effect partially (right).

Deblurring of a motion-blurred image is an *ill-posed inverse problem* [5]. As an example, the image trace of an object moving left to right will be indistinguishable from that of the object moving right to left. Several algorithms have been proposed for extracting motion from blur [2], with various assumptions that eliminate this ill-posedness (such as assuming a known motion profile, constant velocity, constant acceleration, etc.). While these algorithms are effective for image restoration, they are inadequate for accurate dynamics reconstruction since they focus primarily on determining the deblurred image, not the motion field. Furthermore, they are not implementable in real-time because of computational complexity. These drawbacks, while not relevant for image reconstruction, are of prime importance in estimating dynamics for real-time feedback control.

An integrative intensity sensor is unique in that temporal information of the evolution of the output during the exposure time is captured by the sensor, effectively making it a non-linear integral transform. There is scarce literature on modeling sensors as non-linear integral transforms. Bao *et al* [6] modeled the relationship between ocean wave spectra and the corresponding AT-INSAR (along-track interferometric synthetic aperture radar) phase image spectrum measurement as a non-linear integral transform using Gaussian basis functions, which were then approximated as perfect delta functions. This model was not, however, utilized in any dynamic systems framework.

Sandipan Mishra (mishrs2@rpi.edu) is with the faculty of Mechanical, Aerospace, and Nuclear Engineering, Rensselaer Polytechnic Institute, Troy, NY. John Wen (wenj@rpi.edu) is with the faculty of Electrical, Systems and Computer Engineering, Rensselaer Polytechnic Institute, NY.

978-1-61284-799-3/11/$26.00 ©2011 IEEE

It is clear that information in the intensity distribution can be used to estimate the state more accurately through a suitable inversion of the sensor transform. As mentioned earlier, because of the ill-posed-ness of this inverse problem, we require regularization techniques. We propose a regularization that uses the *dynamic model of the underlying system* to remove the ill-posed-ness. Our approach uses a multi-rate extended Kalman filter (EKF) to estimate the state and output evolution during the exposure time from (1) a fast-rate system model, and (2) a slow-rate measurement from an integrative intensity sensor.

To illustrate algorithm development, we present an adaptive optics (AO) system as the target application. AO, i.e., manipulating light wavefronts by dynamically changing optics, was originally proposed in [7] by to correct wavefront errors introduced by atmospheric disturbances in ground based telescopes. Since then, AO has also been used for beam shaping in laser communications [8], confocal microscopes [9], multi-photon microscopes [10], among others.

AO systems use an image sensor to detect wavefront dynamics. The feature that is extracted from this image sensor is a *point object*. The development presented in this paper therefore considers extracting dynamics of point-objects in image sensors. However, the proposed approach can be generalized to extracting dynamics of general (non-rotating) image features.

The paper is organized as follows. Section II presents a brief introduction to AO systems, while Section III defines the scope of the problem considered. Section IV introduces the wavefront sensor (WFS) in the AO system and models it as an integrative intensity sensor. In Section V, the properties of the integrative intensity sensor are exploited for the design of an EKF that utilizes first and second spatial moment information from the intensity distribution obtained from the WFS. Section VI simulates a simplified single-lenslet single-actuator AO system to establish the efficacy of the proposed EKF. Finally, conclusions are drawn in Section VII and a research roadmap is presented.

II. Adaptive Optics System

A typical closed-loop AO configuration (for a telescope) is shown in Figure 2. The actuator in a typical AO system is a MEMS deformable mirror, which can be actuated at fast rates well into the KHz range. In addition to the deformable mirror, the closed loop AO wavefront correction system consists of a wavefront measurement device. There are several types of wavefront sensors (WFS), the most popular of which is the Shack-Hartmann (SH) sensor [11]. The SH sensor measures the local slopes of the wavefront and algorithmically reconstructs the wavefront. It consists of a lenslet array and an imaging device (a CMOS or CCD camera). Typical AO loops use WFS with $10-50$ Hz sampling and 30×30 lenslet arrays. The performance limiting component of the WFS is the image sensor array.

Deformable Mirror Model

The AO deformable mirror-actuator system is often modeled as a uniform membrane with attractive Coulomb force

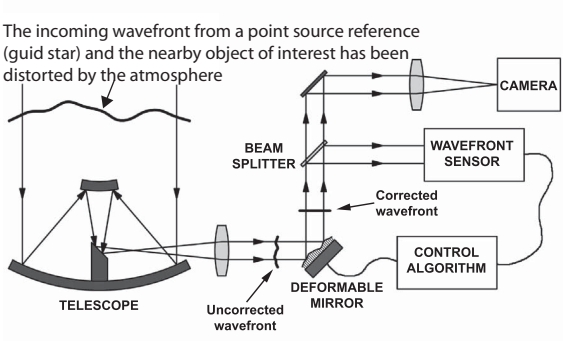

Fig. 2. Adaptive optics for telescope observation

exerted by electrostatic actuators [12]. The non-linear actuator ($u_f(k)=\gamma V_f^2(k)$) is compensated through an inverse-map. The model structure for the mirror-actuator is a standard discrete-time form as shown below, with a (fast) sample time T_f corresponding to the actuator update rate:

$$x_f(k+1)=A_f x_f(k)+B_f u_f(k)+B_w w_f(k) \qquad (1)$$
$$\theta_f(k)=C_f x_f(k)$$

The matrix C_f represents the map from deflection at the actuator locations x_f, to the wavefront slope measurements θ_f.A_f, B_f are functions of the membrane properties and may be obtained by system identification. $u_f(k)$ is the force generated by the actuator, which is $\propto V_f^2(k)$, the applied voltage. Typically T_f is of the order of a few hundred μs.

Wavefront Sensor Model

The wavefront phase slopes ($\theta_f(k)$) are measured by a Shack-Hartmann (SH) WFS. Figure 3 shows a schematic of the sensor. The WFS consists of two key components: (1) a lenslet array (typically grids of 20×20 to 50×50 lenslets) and (2) a CCD/CMOS image sensor. Each lenslet in the array focuses the beam locally onto the image sensor. The *local average* of the slopes of the wavefront at the lenslet, $\theta_x=\frac{x}{L}$ and $\theta_y=\frac{y}{L}$, can be computed from the displacements (x,y) of the beam focus spot from the axis of the lenslet and the focal length of the lenslet L, as shown in Figure 3. The wavefront phase can be reconstructed through a linear operation on the locally averaged slopes at each lenslet.

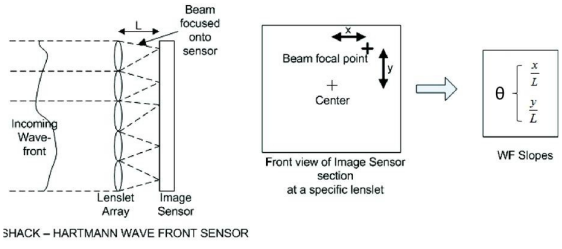

Fig. 3. Schematic of a Shack-Hartmann WFS. The deviation of the focal point from the center of the lenslet (x, y) is directly related to the slopes of the incoming wavefront θ.

In the WFS, each lenslet covers a section of the camera field. Within this section, each pixel location (x,y) corresponds to a particular wavefront slope set ($\theta=[\theta_x \;\; \theta_y]^T$)

in a one-to-one fashion with the x-coordinate determining θ_x and the y-coordinate determining θ_y. Let the wavefront phase slopes of the incoming beam at the p^{th} lenslet be $\theta_{x,p}(\tau)$ and $\theta_{y,p}(\tau)$, for the time instant τ. We now present the development of the WFS as an integrative intensity sensor. The intensity measurement at the camera section corresponding to the p^{th} lenslet is given by (we drop the subscript p for clarity)

$$I(x,y) = \int_{\tau=0}^{T_e} \Psi(x-\theta_x(\tau), y-\theta_y(\tau))\, d\tau + \eta(x,y) \qquad (2)$$

η includes the random and shot noises for the image sensor and T_e is the exposure time.

III. Problem Formulation

Based on the fast-rate actuator model and the image sensor model, we pose the following *state estimation problem*, (P), for the AO system with a fast-rate mirror (updated at T_f) and a slow WFS measurement (updated at $T_e = NT_f$).

$$\begin{aligned} x_f(k+1) &= A_f x_f(k) + B_f u_f(k) + B_w w_f(k) \\ \theta(\tau) &= [\theta_x(\tau) \quad \theta_y(\tau)]^T = Cx(\tau) \\ I(j) &= \int_{(j-1)NT_f}^{jNT_f} \Psi(x-\theta_x(\tau), y-\theta_y(\tau))\, d\tau + \eta(x,y), \\ &\text{where} \quad j = \lfloor \frac{k}{N} \rfloor \end{aligned} \qquad \text{(P)}$$

We pose the problem of estimating x_f at the fast-rate T_f based on measured intensity information $I(j)$ obtained at the slow-rate NT_f.

IV. Integrative Intensity Sensor Model

1-D Intensity Sensor Model

We present the analysis of the WFS as a 1D intensity sensor. The function Ψ (termed the *image kernel*) captures the intensity distribution relating the *spread* of the intensity for a specific wavefront slope set $\theta(\tau)$. For ideal AO systems, Ψ is assumed to be a 2D Dirac delta function: $\Psi(x,y) = \delta(x)\delta(y)$. Since the x and y dependance of Ψ is separable, we can *individually* look at intensities along each axis, x and y, for the corresponding slopes θ_x and θ_y (assuming that the noise η is also separable in x,y). The full coupled 2D case when Ψ is non-separable will be considered in the future.

For ease of notation, we will henceforth denote this single variable as ω (which can take on x or y depending on the slope direction we wish to analyze). This results in an intensity map in the variable ω, as shown below

$$Y(\omega) = \int_{\tau=0}^{T_e} \Psi(\omega - \theta_\omega(\tau))\, d\tau + \eta(\omega) \qquad (3)$$

where $\omega \in \{x,y\}$ This is an example of a unique kind of sensor: ***an integrative intensity sensor***. Based on Eq. (3), these sensors can be interpreted as a non-linear integral transform from the time-doman $\tau \in [0, T_e]$ to the pixel domain ω. Thus, this leads us to believe that output reconstruction *within the exposure time* may be possible from the intensity distribution. But, the inverse transform for the integrative intensity sensor is an ill-posed inverse problem[5]. Therefore, suitable regularization techniques must be used to extract temporal wavefront information from the intensity distribution. In Section V we present an EKF approach, which is essentially a regularization based on the underlying fast-rate dynamic system model.

The Image Kernel

The function $\Psi(x,y)$ establishes the intensity distribution at a given instant τ and is dependent on the irradiance of the source that is generating the intensity distribution. For example, if the sensor is viewing an *image* then $\Psi(x,y)$ captures the image irradiance information. Typically, in image deblurring applications the image kernel is unknown and needs to be identified along with the motion path.

In visual servoing applications, the kernel Ψ can be deduced from the specific feature being tracked, for example, the centroid of an object with *known* shape, an object edge line, etc. For an ideal WFS, this kernel is a point source because of the focusing lenslet, hence modeled as a delta function $\delta(x)\delta(y)$. In an actual WFS, the ideal point source is actually smudged to give an intensity smear which can be approximated by

$$\Psi(\mathbf{x}) = \frac{1}{\sqrt{2\pi|\Sigma|}} e^{-\mathbf{x}^T\Sigma^{-2}\mathbf{x}} \text{ where } \mathbf{x} = [x \quad y]^T \qquad (4)$$

, where $|\cdot|$ represents the determinant. The amount of smear is indicated by the largest singular value of Σ, i.e., $\bar{\sigma}(\Sigma)$.

Time-averaged Output from Intensity Measurement

In Eq.(3), the integration over T_e means that we obtain a *time-averaged* estimate of the intensity profile. Assuming Ψ to be the ideal delta function, we can easily derive the following:

$$\int_{-\infty}^{\infty} \omega Y(\omega) d\omega = \frac{1}{T_e}\int_{\tau=0}^{T_e} \theta_\omega(\tau) d\tau \quad \text{and} \quad \int_{-\infty}^{\infty} Y(\omega) d\omega = 1 \qquad (5)$$

Using the above relationships, the center of gravity y_{CG} (or the first moment) of the intensity distribution is given by

$$\theta_{\omega,ave} = y_{CG} = \frac{\int_{-\infty}^{\infty} \omega Y(\omega) d\omega}{\int_{-\infty}^{\infty} Y(\omega) d\omega} = \frac{1}{T_e}\int_{\tau=0}^{T_e} \theta_\omega(\tau) d\tau \qquad (6)$$

where $\omega \in \{x,y\}$. Therefore, as in typical image processing applications, the center of gravity of the intensity profile is computed to retrieve the time-averaged output ($\theta_{\omega,s}$). We use the subscript s to emphasize that this reading is available at the much slower image update rate ($T_s = T_e$) than the actuator update rate (T_f).

Higher Moments of the Intensity Distribution

Moment computations of intensity distributions have been used frequently in image deblurring algorithms [2], [13]. The p^{th} moment of the univariate intensity distribution in ω is defined as

$$y_p = \frac{\int_{-\infty}^{\infty} \omega^p Y(\omega) d\omega}{\int_{-\infty}^{\infty} Y(\omega) d\omega} \qquad (7)$$

For an image kernel (Ψ) that is a delta function, this higher order moment reduces to $y_p = \frac{1}{T_e}\int_{\tau=0}^{T_e} \theta(\tau)^p d\tau$. Therefore, for this special case, higher spatial moments of the intensity distribution are time-averages of *powers of the output* (θ^p).

It is key to note that the spatial moments are projections of the intensity profile onto the polynomial basis set $\mathscr{B} = \{b_n : b_n(\omega) = \omega^n, n \in Z^+\}$. Alternative basis functions may be designed to improve computational tractability based on the image feature of interest (i.e. the image kernel) and/or the nature of information to be extracted.

In the following sections, we present state estimation schemes for systems with integrative intensity sensor measurements, for the univariate intensity distribution case and assume that the image kernel is $\Psi(\omega) = \delta(\omega)$, a point object. The case of a 2D intensity sensor grid can be developed from extension of these results.

V. State Estimation

Noise Modeling for Integrative Intensity Sensors

In the presence of additive noise at the sensor, the measured intensity distribution at the camera (with exposure time T_e) is given by

$$Y_m(\omega) = \int_{\tau=0}^{T_e} (\Psi(\omega - \theta(\tau)))\, d\tau + \eta(\omega) = Y(\omega) + \eta(\omega) \tag{8}$$

We assume that the noise at each pixel ($\eta(\omega)$) is independent, zero-mean, and Gaussian, with covariance V. Hence, $\mathbf{E}[\eta(\omega)] = 0$ and $\mathbf{E}[\eta(\omega)\eta(\xi)] = V\delta(\omega - \xi)$. Further, we assume that the pixels $\omega \in [-1,1]$ and the output $\theta(\tau) \in [-1,1] \quad \forall\ \tau \in [0, T_e]$.

The (noise-free) center of mass (i.e., the first moment of $Y(\omega)$) is given by

$$\theta_{ave} = y_{CG} = \int_{-1}^{1} \omega Y(\omega) d\omega = \frac{1}{T_e} \int_{\tau=0}^{T_e} \theta(\tau) d\tau \tag{9}$$

In the presence of noise η, using Eqs. 9 and 12, we get

$$\mathbf{E}[y_{CG,m}] = y_{CG} + \mathbf{E}\left[\int_{-1}^{1} \omega\eta(\omega) d\omega\right] = y_{CG} \tag{10}$$

Thus we have no bias in the first moment computation due to noise. To find the covariance of the noise in the first moment,

$$\mathbf{E}\left[(y_{CG,m} - y_{CG})^2\right] = \mathbf{E}\left[\int_{-1}^{1}\int_{-1}^{1} \omega\xi\eta(\omega)\eta(\xi) d\omega d\xi\right] = \frac{2}{3}V.$$

Following a similar procedure, we can also show that for the second moment

$$\mathbf{E}[y_{2,m}] = y_2 \quad \text{and} \quad \mathbf{E}\left[(y_{2,m} - y_2)^2\right] = \frac{2}{5}V. \tag{11}$$

Finally, we show that the cross-covariance terms $\mathbf{E}[(y_{1,m} - y_1)(y_{2,m} - y_2)]$ are zero.

Discrete-time Estimation

Since the estimation and control algorithms are designed in discrete time, we may approximate the moment equation, Eq. (7) as a finite sum with a sampling time T_f, and $N = \frac{T_e}{T_f}$.

$$y_p = \frac{1}{N} \sum_{i=0}^{N-1} \left(C_f A_f^i x_f(k)\right)^p \tag{12}$$

Therefore, we have the following lifted system description when we use the first moment ($p = 1$) as the only output measurement

$$\begin{aligned} x_f(k+N) &= A_f^N x_f(k) + B_w w(k) \\ y_{1,m}(k+N) &= \bar{C} x_f(k) + n_1(k), \\ = \frac{1}{N}\left[C_f + C_f A_f + \ldots + C_f A_f^{N-1}\right] x_f(k) &+ n_1(k), \\ w \sim \mathscr{N}(0,W) \qquad n_1 &\sim \mathscr{N}\left(0, \frac{2}{3}V\right) \end{aligned}$$

where the process noise is $B_w w(k)$ and the measurement noise is $n_1(k)$.

Remark 1: It is easy to show that $\left(A_f^N, \bar{C}\right)$ is an observable pair if $\left(A_f, C_f\right)$ is observable.

Using only the center of mass of the intensity distribution means that we are throwing away quite a bit of information available in the sensor measurement. For example, by using the second moment of the intensity distribution, we have an additional output equation

$$\begin{aligned} y_{2,m}(k+N) = \quad & h(x_f(k)) + n_2(k), \quad n_2 \sim \mathscr{N}\left(0, \tfrac{2}{5}V\right) \\ = \quad & \frac{1}{N}\sum_{i=0}^{N-1} \left(CA^i x_f(k)\right)^2 + n_2(k) \end{aligned} \tag{13}$$

Thus, we now have a non-linear output ($y_{2,m}$) in addition to the linear output($y_{1,m}$).

Remark 2: This is a Wiener system with a static non-linearity on the output of a polynomial form. Conditions for these Wiener systems developed in [14] established that the system is *detectable from the non-linear output* ($y_{2,m}$) if $\rho(\bar{A}) < 1$ and $\left(\bar{A}, \bar{C}\right)$ is observable.

We approximate the probability distributions of n_1 and n_2 jointly using their second order statistics (mean and covariance) assuming a Gaussian distribution. Thus, the overall lifted system description becomes:

$$\begin{aligned} x_f(k+N) = \quad & A_f^N x_f(k) + B_w w(k) \qquad w \sim \mathscr{N}(0,W) \\ y_{1,m}(k+N) = \quad & \bar{C} x_f(k) + n_1(k) \\ y_{2,m}(k+N) = \quad & h(x_f(k)) + n_2(k) \\ & \begin{bmatrix} n_1 \\ n_2 \end{bmatrix} \sim \mathscr{N}\left(\begin{bmatrix} 0 \\ 0 \end{bmatrix}, \begin{bmatrix} \frac{2}{3}V & 0 \\ 0 & \frac{2}{5}V \end{bmatrix}\right) \end{aligned} \tag{14}$$

Remark 3: Using the additional non-linear output can achieve a smaller (or equal) estimation error covariance. From the definition of conditional expectation, the optimal estimator using y_1 and y_2 delivers estimation error covariance lesser than or equal to the optimal estimator that uses only y_1. Therefore, next we design an extended Kalman filter (EKF) [15] using the two outputs to exploit the second moment information obtained from the image sensor.

Extended Kalman Filter Estimation

For the system described above, we then use the following EKF as the state estimator [15]. Since measurements are received every N steps, we will introduce the index j, which increments by 1 every N time steps. The *local linearization,* H_j of the nonlinear output y_2 is given by

$$H_j = \frac{\partial y_2(j)}{\partial x_f(j)}|_{x_{j|j-1}} = \frac{2}{N}\sum_{i=0}^{N-1} x_{j|j-1}^T \left(C_f A_f^i\right)^T \left(C_f A_f^i\right) \tag{15}$$

We use this local linearization for the EKF estimation as shown below:

$$\text{Prediction:} \quad \hat{x}_{j|j-1} = A_f^N \hat{x}_{j-1|j-1} \tag{16}$$

$$P_{j|j-1} = A_f^N P_{j-1|j-1} (A_f^N)^T + B_w W B_w^T \tag{17}$$

$$\text{Kalman Gain:} \quad K_j = P_{j|j-1} \begin{bmatrix} \bar{C} \\ H_j \end{bmatrix} \left(\begin{bmatrix} \frac{2}{3}V & 0 \\ 0 & \frac{2}{5}V \end{bmatrix} + \begin{bmatrix} \bar{C} \\ H_j \end{bmatrix} P_{j|j-1} \begin{bmatrix} \bar{C}^T & H_j^T \end{bmatrix} \right)^{-1} \tag{18}$$

$$\text{Correction:} \quad P_{j|j} = P_{j|j-1} - K_j \begin{bmatrix} \bar{C} \\ H_j \end{bmatrix} P_{j|j-1} \tag{19}$$

$$\hat{x}_{j|j} = \hat{x}_{j|j-1} + K_j \left(\begin{bmatrix} y_{1,m}(j) \\ y_{2,m}(j) \end{bmatrix} - \begin{bmatrix} \bar{C} \\ H_j \end{bmatrix} \hat{x}_{j|j-1} \right) \tag{20}$$

It is interesting to note that since H_j and $\bar{C}$ are locally independent, we may entertain the possibility of constructing a passive output y_P as a combination of the two outputs y_1 and y_2. This passive output can then be used for a robust feedback controller.

VI. Simulated Example

We now present an example to illustrate the EKF scheme developed in the previous section.

System Model

The underlying discrete-time fast-rate system (with sampling rate $T_f = 1$ms corresponding to the actuator update rate) is given by the following model

$$x_f(k+1) = \begin{bmatrix} 1.0000 & 0.0010 \\ -0.0197 & 0.9704 \end{bmatrix} x_f(k) + \begin{bmatrix} 0 \\ 1 \end{bmatrix} u_f(k) + \begin{bmatrix} 0 \\ 0.05 \end{bmatrix} w_f(k) \tag{21}$$

$$\theta_f(k) = \begin{bmatrix} 0.001 & 0 \end{bmatrix} x_f(k) \tag{22}$$

The exposure time is $T_e = 200$ms, i.e., we get an intensity distribution measurement every $N = 200$ fast-rate steps. The intensity distribution is assumed to be generated by a Gaussian image kernel $\Psi(\omega - \theta(t)) = \frac{1}{\sqrt{2\pi\sigma}} e^{-\frac{(\omega-\theta(t))^2}{\sigma^2}}$ with $\sigma = 0.05$ ($\sigma = 0$ corresponds to a delta function). A small σ results in a small smudging of the perfectly sharp intensity distribution.

The additive random noise in the image intensity distribution η is white, zero mean, and with covariance $V = 0.1$ (This corresponds to a signal to noise ratio of 0.05 at the photodetector for the CMOS element). The effect of the process noise $w_f(k) \in \Re$ over N steps is $w(j) \in \Re$, with zero mean and covariance $W = \bar{B} W_f \bar{B}^T = 0.1$.

Observer Design Scenarios

We compare three design scenarios: **(O1)** A steady state Kalman filter designed based on the lifted system $\bar{A}, \bar{B}$ and the noise covariances V and W, using *only* the first moment (y_1) of the intensity distribution, **(O2)** an EKF designed based on the lifted system $\bar{A}, \bar{B}$ and the noise covariances V and W, using *only* the second moment (y_2) of the intensity distribution and **(O3)** the EKF observer designed in the previous section based on the lifted system $\bar{A}, \bar{B}$ and the noise covariances V and W, using both the first and second moments (y_1, y_2) of the measured intensity distribution. Note that the measurements are available only every N fast-rate steps. To account for the input u_f, the predictor equations for the observers are modified as $\hat{x}_{j|j-1} = A_f^N \hat{x}_{j-1|j-1} + \sum_{i=0}^{N-1} A_f^i B_f u_f(jN - i)$.

Results

Figure 4 shows a comparison of the estimated state $\hat{x}_{f,1} = \hat{\theta}$ using (1) a measurement of the first moment y_1 *only* (**O1**) and (2) a measurement of the second moment y_2 *only* (**O2**). We observe that state estimation is possible by using either y_1 or y_2 since in both cases the estimates converge to the true state. This corroborates our claim that the lifted system is observable from y_1 as well as the non-linear output y_2.

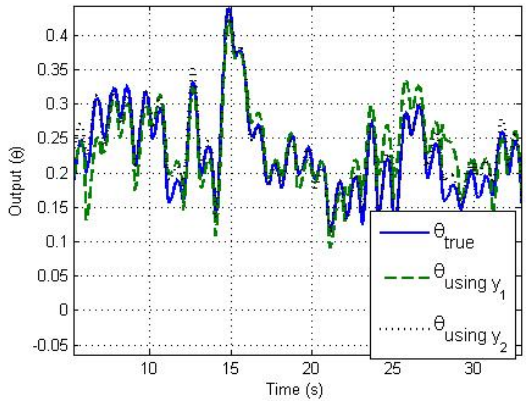

Fig. 4. Estimation of the state variable $x_{f,1} = \theta_f$ using (dashed) a measurement of the first moment y_1 only (**O1**) and (dotted) a measurement of the second moment y_2 only (**O2**).

Next, we use the EKF scheme **O3** (which uses both y_1 and y_2) derived in Section V for state estimation and compare to the steady state KF **O1** (which uses only the linear output y_1). Figure 5 shows the state estimation error norm ($\|\hat{x}_{j|j} - x(j)\|_2$) plotted against the time step j. It is evident that the EKF delivers a lower steady-state estimation error covariance (~ 0.05) as compared to the KF (~ 0.07). Figure 6 shows the error in estimation of the wavefront slope θ_f at the fast-rate for a section of the simulation time. Therefore, using the additional non-linear output y_2 can improve the estimation of the output, particularly in the presence of significant process noise. Finally, in Figure 7, a zoomed-in detail of the estimate and actual output *within* a single exposure of the image sensor is shown, highlighting the fact that we have a multi-rate estimation scheme that has better inter-sample behavior.

VII. Conclusions and Future Work

Image sensors are now widely being used as feedback mechanisms. These sensors, essentially CCD or CMOS camera elements, fall into a unique class of integrative intensity sensors. Typically, the image sensors are slow and outputs are estimated by finding the center of mass (the first moment) of the intensity distribution, which corresponds to the temporal average of the output profile over the exposure period of the

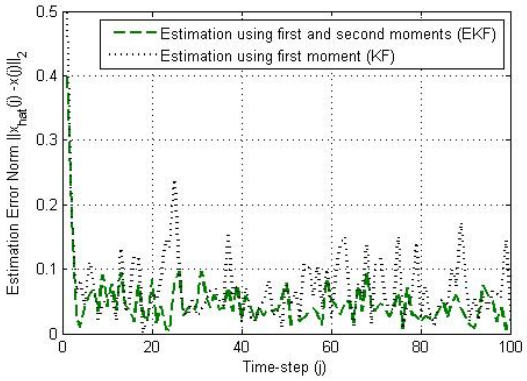

Fig. 5. State estimation error norm ($\|\hat{x}_{j|j} - x(j)\|_2$) plotted against the time step j using (1, dotted) a measurement of the first moment ($y_{1,m}$) only through a KF (**O1**) and (2, dashed) combining the first and second moment measurements y_1, y_2 using the EKF (**O3**).

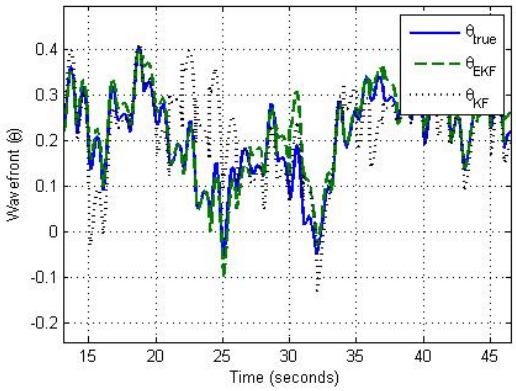

Fig. 6. Estimation of the state variable $x_{f,1} = \theta_f$ using using (1, dotted) a measurement of the first moment (y_1) only through a KF (**O1**) and (2, dashed) combining the first and second moment measurements y_1, y_2 using the EKF (**O3**).

image sensor. The intensity blur is considered undesirable and discarded through this averaging. However, substantial temporal information about the output is encoded in the intensity blur and may be used for a better state estimate.

Thus, a model was developed for the class of integrative intensity sensors. The integrative intensity sensor is effectively a non-linear integral transform from time-domain evolution of the output to a pixel-domain intensity distribution that captures the relative length of time for which the output resides at a given value. Thus, additional information (about the output) in the form of higher moments of the intensity distribution were obtained from these sensors. Observability of the system from first and second moments of the intensity distribution was established. In addition, an EKF that used the first and second moments for state estimation was proposed and was shown to outperform a standard KF using only the first moment.

This research opens up the potential for several exciting possiblities for applications that use image sensors, such as system identification using integrative sensors, robust inverse transforms for integrative sensors, and dynamic control of exposure time as a means of extracting more information from such sensors.

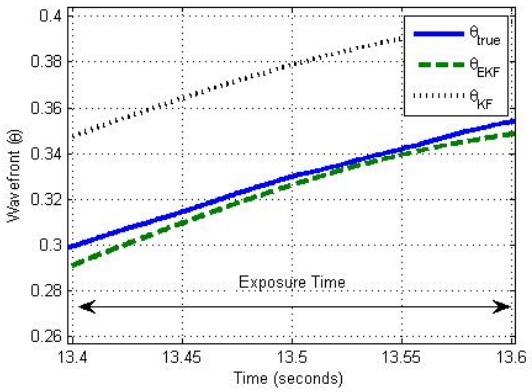

Fig. 7. Zoomed-in detail of estimation of the output *within* a single exposure (i.e., in between measurements).

REFERENCES

[1] D. Glasson, "Development and applications of multirate digital control," *Control Systems Magazine, IEEE*, vol. 3, no. 4, pp. 2 – 8, 1983.

[2] W.-G. Chen, N. Nandhakumar, and W. N. Martin, "Image motion estimation from motion smear-a new computational model," *Pattern Analysis and Machine Intelligence, IEEE Transactions on*, vol. 18, pp. 412–425, 1996.

[3] Q. Shan, J. Jia, and A. Agarwala, "High-quality motion deblurring from a single image," in *ACM SIGGRAPH 2008 papers*, ser. SIGGRAPH '08, 2008, pp. 73:1–73:10.

[4] S. Hammett, "Motion blur and motion sharpening in the human visual system," *Vision Research*, vol. 37, no. 18, pp. 2505 – 2510, 1997.

[5] J. Biemond, R. Lagendijk, and R. Mersereau, "Iterative methods for image deblurring," *Proceedings of the IEEE*, vol. 78, no. 5, pp. 856 –883, May 1990.

[6] M. Bao, W. Alpers, and C. Bruning, "A new nonlinear integral transform relating ocean wave spectra to phase image spectra of an along-track interferometric synthetic aperture radar," *Geoscience and Remote Sensing, IEEE Transactions on*, vol. 37, Jan. 1999.

[7] H. W. Babcock, "The possibility of compensating astronimical seeing," *Astronomical society of the pacific*, vol. 65, no. 386, pp. 229–236, 1952.

[8] R. K. Tyson and D. E. Canning, "Bit-error rate improvement of a laser communication system with low-order adaptive optics," in *Proc. SPIE, Free-Space Laser Communication and Laser Imaging II,*, 2002, pp. 82–87.

[9] S. P. Poland, D. Burns, W. Lubeigt, B. A. Patterson, G. Valentine, A. J. Wright, and J. M. Girkin, "Use of optimisation algorithmic techniques with active optics for aberration correction in optical sectioning microscopy," W. Jiang, Ed., vol. 6018, no. 1. SPIE, 2005, p. 60181H. [Online]. Available: http://link.aip.org/link/?PSI/6018/60181H/1

[10] J. M. Girkin and P. N. Marsh, "Use of adaptive optics for improved multiphoton imaging," A. Periasamy and P. T. C. So, Eds., vol. 5323, no. 1. SPIE, 2004, pp. 260–266. [Online]. Available: http://link.aip.org/link/?PSI/5323/260/1

[11] B. C. Platt and R. Shack, "History and principles of shack-hartmann wavefront sensing." *Journal of Refractive Surgery*, vol. 17, no. 5, pp. 573–577, 2001.

[12] N. Doble and D. Miller, "Wavefront correctors for vision scinece," in *Adaptive Optics for Vision Science*, J. Porter, H. Queener, J. Lin, K. thorn, and A. Awwal, Eds. Wiley, 2006, pp. 83–117.

[13] Y. Zhang, C. Wen, and Y. Zhang, "Estimation of motion parameters from blurred images," *Pattern Recognition Letters*, vol. 21, no. 5, pp. 425 – 433, 2000.

[14] D. Nesic, "Observability for simple Wiener and simple Wiener-Hammerstein systems," in *American Control Conference, 1998. Proceedings of the 1998*, vol. 4, June 1998, pp. 2349 –2353.

[15] E. Wan and R. Van Der Merwe, "The unscented Kalman filter for nonlinear estimation," in *Adaptive Systems for Signal Processing, Communications, and Control Symposium 2000. AS-SPCC. The IEEE 2000*, 2000.